Physical properties of NEOs derived from their phase curves

Plícida Arcoverde [1]★ Eduardo Rondón [1], Filipe Monteiro [1], Weslley Pereira,[1] Simone Ieva [2],
Tatiana Michtchenko,[3] Marçal Evangelista-Santana,[1] Jonatan Michimani,[1] Wesley Mesquita,[1]
Tatiane Corrêa,[1] Elisabetta Dotto,[2] Alessio Giunta,[2] Andrea Di Paola,[2] Hissa Medeiros [1,4]
Jorge M. Carvano,[1] Teresinha Rodrigues[1] and Daniela Lazzaro [1]

[1]*Observatório Nacional, Rua Gal. José Cristino 77, 20921-400 Rio de Janeiro, Brazil*
[2]*INAF − Osservatorio Astronomico di Roma, via Frascati 33, I-00078 Monteporzio Catone (Roma), Italy*
[3]*Universidade de São Paulo, IAG, Rua do Matão 1226, Cidade Universitária, 05508-090 São Paulo, Brasil*
[4]*Instituto de Astrofísica de Canarias (IAC), C/Vía Láctea sn, E-38205 La Laguna, Spain*

ABSTRACT

The observation of Near Earth objects (NEOs) allows us to study the physical properties of the smallest size bodies of our Solar System and help impose constraints on their origin and evolution. The solar phase curve is a very important tool to derive diverse physical properties of a small body so that we set up an observational campaign to derive the phase curve parameters (H, G_1, G_2) for a large number of NEOs. We present here the obtained phase curves for 12 NEOs, along with the rotation period for two of them and the V–R colour for four. The data was acquired mainly at the Astronomical Observatory of Sertão de Itaparica (Brazil), with some NEOs also observed at the Osservatorio di Campo Imperatore (Italy). Considering all the objects observed throughout our campaign we analysed a homogeneous dataset of 30 NEOs along with data acquired by ATLAS (Asteroid Terrestrial-impact Last Alert System telescopes survey) for MB asteroids. The behavior in the phase space G_1-G_2 of 21,865 MBA and 103 NEOs was analysed, separating the objects in intervals of albedos and sizes. From the large MB data set we found evidence that the distribution in the G_1-G_2 phase space has strong dependence not only on the albedo but also on the object's size. This is particularly true for the smaller objects. The main result being that, on the contrary to what occurs with the MB larger objects, we are unable to estimate the albedo of a NEO from its phase curve parameters.

Key words: methods: data analysis – methods: observational – techniques: photometric – minor planets, asteroids: general.

1 INTRODUCTION

The study of the different physical properties of small bodies in the Solar System provides a better understanding on how they are distributed within the different populations. These distributions, in turn, allow us to obtain important information about the physical processes that are acting, or that acted in the past, and to impose constraints to the formation and evolution models of our planetary system.

Near Earth objects (NEOs), which can be asteroids or comets, form a particularly interesting population to study (e.g. Binzel, Reddy & Dunn 2015). Considering that these objects are in unstable orbits over the age of the Solar System, this implies that it is a transient population, whose main source is estimated to be the innermost regions of the Main Belt (MB) of asteroids (Michel et al. 2000; Bottke et al. 2002; Morbidelli et al. 2015). Therefore, several studies are being carried on to confirm this hypothesis and to identify the most probable regions which deliver the NEOs to their current location. One approach is the comparison of the physical properties of different populations.

Important physical properties of atmosphereless bodies can be derived from their phase curves which represent how the object's brightness varies with the solar phase angle. These properties are based on the understanding that the physical properties of the material present on the object's surface can be retrieved from the analysis of the scattering of the incident solar radiation. In particular, properties related to the composition, texture, and roughness can be determined (Hapke 1981, 1984, 1986; Lumme & Bowell 1981; Helfenstein & Veverka 1989).

The current models that describe the phase curve of atmosphereless objects, adopted by the IAU since 2010, are the H-G_1–G_2 and the H-G_{12} (Muinonen et al. 2010; Penttilä et al. 2016). In Penttilä et al. (2016) it is suggested a constrained non-linear least-squares method for the three-parameter model H-G_1–G_2, to ensure a good phase curve fit even with few data. On the other hand, in cases with a good coverage, the two methods are equivalent, there is no restriction between the linear and non-linear methods.

The absolute magnitude, H_0, is defined as the reduced magnitude at zero solar phase angle, and is fundamental to correctly determine the diameter of a body, when its albedo is known. On the other hand, the slope parameters, G_1–G_2, give information on the albedo, taxonomic type, surface roughness, and porosity (Belskaya & Shevchenko 2000; Warner, Harris & Pravec 2009; Shevchenko et al. 2016). It

is important to note that in order to have a reliable determination of these parameters, it is necessary a good coverage in terms of phase angles, the best being between nearly 0° and 30–35°. The most crucial region is between 0° and ∼8°, where it take place the opposition effect (OE). This phenomenon is characterized by the exponential increase in brightness of objects without atmosphere caused by shadowing-mechanism and coherent-backscattering effects (e.g. Irvine 1966; Hapke 1981; Mishchenko 1992; Mishchenko & Dlugach 1992; Shkuratov et al. 1999; Belskaya & Shevchenko 2000; Mishchenko et al. 2009; Muinonen et al. 2012; Morozhenko & Vidmachenko 2013).

With the aim to obtain physical parameters of NEOs since 2017 we set up an observational campaign to derive phase curves of these objects (Rondón et al. 2019, 2022; and Ieva et al. 2022), and here we present the results for 12 NEOs. The total sample of 30 acquired by the observing campaign was then used to perform a comparative study between the phase curve parameters of NEOs and objects from the MB.

The present work is organized as follows: in Section 2 we describe the observations and data reduction, as well as the methodology used to derive the phase curve parameters. In Section 3 we present and discuss the results for each NEO separately. In Section 4 we first describe the databases used to compare NEOs with MB objects and then perform several analysis searching for trends that can help derive physical information on a body from its phase curve parameters.

2 OBSERVATIONS

2.1 Observations and data reduction

The data to derive the NEOs phase curves was mostly obtained at the *Observatório Astronômico do Sertão de Itaparica* (OASI, Brazil), within the framework of the IMPACTON project (Lazzaro 2010; Rondón et al. 2020). The observations were performed using the 1-m telescope and two CCD cameras with different pixel arrays, one of 1024 × 1024 and the other of 2048 × 2048 [details on the available instrumentation at OASI are given in Rondón et al. (2020)]. The R and V Johnson-Cousins filters were used to obtain the data, which occurred between 2016 September and 2021 March.

To obtain the reduced magnitude at different solar phase angles, thus the phase curve, we observed our target and a Landolt standard star three or four times over the night. At each time, four or more images were obtained, and the resulting magnitudes were then averaged to reduce the random error. The whole procedure was repeated on different nights over one or more months to map different solar phase angles of the NEO. The data reduction was performed using Image Reduction and Analysis Facility (IRAF) software, correcting the science image by bias, dark, and flat frames. Through these corrected images we determined the instrumental magnitudes and their errors for the asteroid and the standard star using aperture photometry through growth curve (Howell 1989).

The asteroid's reduced magnitude is obtained using standard procedures: first correcting the asteroid and standard star instrumental magnitudes for the atmospheric effects, then computing the calibrated magnitude using the tabulated value for the standard star (Landolt 1992) and finally setting the asteroid to a distance of 1 AU from Earth and the Sun. This reduced magnitude is the $H(\alpha)$ given in equation (1) below. In each of the above steps the associated error is propagated to determine the final error in the reduced magnitude.

In order to determine the phase curve corrected by the object's rotation, as explained in the next section, it was also necessary to obtain simultaneously its light curve. The light curve was determined

by observing the target over several hours per night. The light curve was then obtained using standard procedures to derive relative or reduced magnitudes, and the period determined by a Fourier fit (Harris et al. 1989). The MPO Canopus software (Warner 2019) was used to determine the rotational periods.

Some NEOs were also observed at the Osservatorio di Campo Imperatore (CI, Italy). The observations were performed using the 0.9-m *Schmidt Telescope* equipped with a 4096 × 4096 CCD covering a field of view of 1.15 × 1.15 square degrees and a scale of 1 arcsec per pixel. A Sloan Digital Sky Survey (SDSS) r filter was used in all observations obtained between 2016 May and 2017 June. For these observations were applied standard reduction techniques and was also necessary to transform the reduced magnitudes to the R-Cousins filter as described in Ieva et al. (2022).

For each NEO, the observational conditions are given in Table 1 while the derived reduced magnitudes, and associated error, in Table A1 of the Appendix.

2.2 Parameters determination

Since 2010 the IAU adopted the three parameters model H-G_1–G_2 developed by Muinonen et al. (2010) as the standard fit for solar phase curve modeling. However, when the number of observations is small or when the data has low precision, the fit fails. Penttilä et al. (2016) solve this problem using a restricted non-linear least-squares algorithm to fit the data to the model providing a good prediction of the phase curve parameters even for low precision data. Since our data was obtained at spaced intervals and sometimes with few observations we, thus, used this approach with the curve parameters given by the equation,

$$H(\alpha) = H_0 - 2.5 \log_{10}[(G_1\Phi_1(\alpha) + G_2\Phi_2(\alpha) + (1 - G_1 - G_2)\Phi3(\alpha)], \quad (1)$$

where α is the phase angle, $H(\alpha)$ is the reduced magnitude, H_0 is the absolute magnitude, G_1 and G_2 are the slope parameters, and the base functions Φ_1, Φ_2, and Φ_3 are cubic splines functions. Before fitting the model to our data it is important to note that the solar phase curve is highly affected by the shape of the object, especially if this is elongated. The elongated shape of an asteroid can cause large variations, or amplitude, of the light curve which can lead to significant differences between the magnitude determined at the minimum or at the maximum. These variation result in fluctuations of the phase curve points with large influence on the errors of the fit.

To correct this effect, it is necessary to obtain the light curve of the asteroid at the same time in which the data of the phase curve is taken, or very near it. Then, using the procedure described in Rondón et al. (2019), we extrapolated the rotational light curve to the dates of our phase curve observations and obtained a nominal correction, $\Delta V'(\phi)$, to be applied to the reduced magnitude $H(\alpha)$, deriving the corrected magnitude, $H'_c(\alpha)$, as shown in the equation bellow,

$$V'(\phi) = AV(\phi + \phi_0) \quad (2)$$

$$H'_c(\alpha) = H(\alpha) - \Delta V'(\phi). \quad (3)$$

In the above equations V and V' are the rotational light curve function at rotational phase $\phi + \phi_0$ and at ϕ, respectively. A is the amplitude ratio of the rotational light curve as defined by Zappala et al. (1990). $H(\alpha)$ and $H'_c(\alpha)$ are the reduced and corrected magnitudes at solar phase α, respectively. The corrected magnitudes

Table 1. For each observed NEO is given the name, the period of observation, the solar phase angle interval, the albedo, the taxonomic type, when available, the rotation period, and light-curve amplitude used for correction.

Asteroid	Group	Observation period	Phase angle interval (°)	Albedo[1] p_v	Tax. type	Period (h)	Amplitude (mag)
(4055) Magellan	Amor	02/2017–03/2017	3.0–13.7	0.330	V[2]	7.52[3]	0.38
(18109) 2000 NG11	Amor	02/2018–10/2018	3.4–34.8	–	C[4]/X[5]	4.252[6]	0.84
(65717) 1993 BX3	Apollo (PHA)	02/2021–03/2021	7.9–34.7	0.15[7]	–	20.331[8]	0.83
(99799) 2002 LJ3	Amor	08/2018–12/2018	8.6–62.3	0.43[9,10]	Sq[11]/S[5]/Q[2]	2.64[6]	0.23
(174050) 2002 CC19	Amor	02/2021–02/2021	6.2–35.4	–	–	4.2344	0.181
(175189) 2005 EC224	Amor	12/2016–06/2020	0.7–36.6	0.204[12]	–	3.75[13]	0.15
(417581) 2006 VA3	Apollo	02/2021–02/2021	11.3–81	0.145[14]	–	5.481[6]	0.40
(464797) 2004 FZ1	Apollo	08/2016–08/2016	8.7–18.9	0.103[14]	Sr[2]	45.4[15]	0.39
(480004) 2014 KD91	Amor	09/2016–10/2016	14.8–26.6	0.125[14]	–	2.835[6]	0.17
2011 YQ10	Amor	10/2021–12/2021	5.7–48.3	–	–	4.8651	0.096
2016 RP33	Amor	09/2016–09/2016	7.6–18.3	–	–	4.707[16]	0.22
2017 AC5	Amor	02/2017–03/2017	5.4–18.8	–	S[17]	5.922[3]	0.81

References; (1) Mainzer et al. (2011), (2) Binzel et al. (2019), (3) Warner (2017b), (4) Dandy, Fitzsimmons & Collander-Brown (2003), (5) Carry et al. (2016), (6) Monteiro et al. (2023), (7) Lin et al. (2018), (8) Warner & Stephens (2021), (9) Mueller et al. (2011), (10) Trilling et al. (2010), (11) Thomas et al. (2014), (12) Masiero et al. (2020a), (13) Warner & Stephens (2020), (14) Masiero et al. (2020b), (15) Warner (2017a), (16) Monteiro et al. (2018), (17) Ieva et al. (2020).

compose and minimize the dispersion of the curve. It is important to note, that in some cases we used data from the MPC database (https://alcdef.org/) when this was obtained near the time of our observations. It is important to note that we did not propagated the rotational curve error to derive the final error in the H and G_1–G_2 parameters. This was done mainly to maintain homogeneity, since we used several results from the literature, when this error is not given.

Once the absolute magnitude, the V–R colour and the visible albedo are known, it is possible also to determine the diameter of the object using equation (4) (Tedesco et al. 1992; Harris & Lagerros 2002; Muinonen et al. 2010; Rondón et al. 2019). In our case, we use visual albedo values (p_v) from Mainzer et al. (2011) for those NEOs for which we derived the V–R colour, since the absolute magnitude is obtained in the R-Cousins filter (H_{0R}),

$$D = \frac{1329 \cdot 10^{-\frac{1}{5}(H_{0R}+V-R)}}{\sqrt{p_v}}. \quad (4)$$

However, this value must be taken with care as both albedo and diameter are obtained together by NEOWISE. In Table 1 for each of the 12 observed NEOs is given, the name, the group, the period of observation, and the solar phase interval. Whenever available, the albedo from NEOWISE (Mainzer et al. 2011) is also given, the taxonomic classification derived by different authors, as well as the period rotation and light-curve amplitude. The obtained corrected magnitudes are given in Table A2 of the Appendix.

3 RESULTS

3.1 NEOs phase curves

In this work we derived phase curves for twelve NEOs, nine belonging to the Amor group – (4055) Magellan, (18109) 2000 NG11, (99799) 2002 LJ3, (174050) 2002 CC19, (175189) 2005 EC224, (480004) 2014 KD91, 2011 YQ10, 2016 RP33, 2017 AC5 – and three to the Apollo group – (65717) 1993 BX3, (417581) 2006 VA3, and (464797) 2004 FZ1. Among these, (65717) 1993 BX3 is also classified as Potentially Hazardous Asteroids (PHA). For four NEOs, (65717) 1993 BX3, (174050) 2002 CC19, (417581) 2006 VA3, and 2011 YQ10, we also obtained their V–R colour.

The numerical procedure used to fit the data and derive the absolute magnitudes and the G_1–G_2 parameters is a PYTHON code described by Penttilä et al. (2016) and available on the online platform 'Online Calculator for H, G1, G2 photometric system (OCP)'.[1] The code give also the error associated to each derived parameter. In Table 2 are given the derived absolute magnitudes and slope parameters with their respective errors, the fit error (fit_{err}), as well as the V–R colour and the diameter for some asteroids, with respective date and phase angle at which it were acquired. It is important to highlight here that asteroids can undergo phase reddening (Sanchez et al. 2012), meaning that colours computed at $\alpha > 0°$ may be different to those at $\alpha = 0°$, thus, introducing an uncertainty in the diameter determination. However, for $\alpha < 30°$, as in the present work, the phase reddening is minimized and the colours variation is very small Sanchez et al. (2012). Note that the fit_{err} is computed as a measure of the dispersion function extrapolated to $\alpha = 0$, while the H_{err} is the uncertainty in H_{0R}. The obtained phase curves, with respective fit to the H-G_1–G_2 model, will be shown and discussed below for each one of the observed NEO.

3.1.1 (4055) Magellan

Classified as a V-type (Sanchez et al. 2013; Thomas et al. 2014; Vereš et al. 2015; Carry et al. 2016; Lin et al. 2018; Binzel et al. 2019), this NEO, belonging to the Amor group, was observed only at CI between 2017 February and March. With an albedo of $p_v = 0.330$ and a diameter of $D = 2.781$ km determined by Mainzer et al. (2011), this NEO had a phase angle coverage from 3.0° to 13.7°, and the derived magnitude and absolute slope parameters are $H_{0R} = 13.94$, $G_1 = 0.07041$ and $G_2 = 0.3724$. Fig. 1 shows the phase curve, which seem to indicates a large opposition surge, however, driven by just one point in this region so that more data is needed to confirm this result. The lack of data at smaller phase angle is also responsible for the large error, of about 1 mag, in the H_{0R} value (Table 2). On the other hand, the fit has a small error, ±0.188, which is due to the small individual magnitude errors as well as to the use of the restricted non-linear least-squares algorithm by Penttilä et al. (2016).

[1]http://h152.it.helsinki.fi/HG1G2/

Table 2. Determined parameter for 12 NEOs observed at OASI and CI.

Asteroid	H_{0R}	H_{0Rerr}	G_1	G_{1err}	G_2	G_{2err}	fit_{err}
(4055) Magellan	13.94	−1.23 +0.85	0.07041	−0.0722 +0.0929	0.3724	−0.335 +0.5273	±0.188
(18109) 2000 NG11	16.53	−0.08 +0.62	0.8301	−0.2413 +0.048	0.01628	−0.0 +0.4196	±0.01
(65717) 1993 BX3	20.45	−0.18 +0.47	0.9662	−0.3761 +0.0207	0.0	−0.0 +0.4091	±0.199
(99799) 2002 LJ3	18.21	−0.46 0.22	0.7792	−0.1462 +0.0182	0.2208	−0.2539 +0.1456	±0.07
(174050) 2002 CC19	16.626	−0.234 +0.241	0.0	−0.0 +0.0731	0.1919	−0.0475 +0.0655	±0.377
(175189) 2005 EC224	18.07	−1.14 +0.179	0.3626	−0.0 +0.1679	0.343	−0.0 +0.480	±0.148
(417581) 2006 VA3	17.37	−0.41 +0.21	0.7687	−0.2397 +0.2298	0.2313	−0.0273 +0.2346	±0.055
(464797) 2004 FZ1	17.39	−0.92 +0.62	0.2593	−0.0693 +0.3836	0.3831	−0.0405 +0.2917	±0.091
(480004) 2014 KD91	16.96	−0.36 +0.67	0.2613	−0.007 +0.0534	0.3499	−0.0056 +0.136	±0.328
2011 YQ10	18.844	−0.322 +0.285	0.6749	−0.2153 +0.009	0.3251	−0.2395 +0.2167	±0.012
2016 RP33	18.331	−0.619 +0.603	0.1609	−0.0291 +0.0414	0.1418	−0.1288 +0.2355	±0.229
2017 AC5	20.01	−1.25 +1.47	0.819	−0.057 +0.0	0.0	−0.0 +0.9755	±0.178

Asteroid	V–R	date	α (°)	D (km)	D_{err}
(65717) 1993 BX3	0.484	2021/03/13	7.9	0.223	0.169
(174050) 2002 CC19	0.231	2021/02/11	35.4	−	−
(417581) 2006 VA3	0.435	2021/02/11	26.3	0.959	0.283
2011 YQ10	0.496	2021/10/05	47.7	−	−

In the upper part are given the phase curve parameters where the columns indicate the asteroid name, the absolute magnitude (H_{R0}), the slope parameters (G_1 and G_2), with their respective errors, and the fit error (fit_{err}). In the lower part are given the V–R colours derived for four objects along with the date, phase angle at which the colour was acquired and the diameter for those with previously determined albedo.
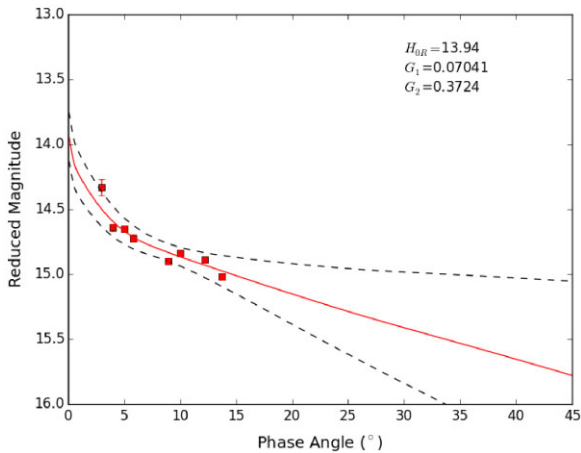

Figure 1. Phase curve of the NEO (4055) Magellan. The points are the corrected reduced magnitudes, with respective errors, while the lines indicate the best fit to the H-G_1–G_2 model and the envelope error.

The rotation period for this NEO was determined by several authors (Erasmus et al. 2017; Vaduvescu et al. 2017; Warner 2017b; Pravec 2019; Ieva et al. 2020). However, to correct our magnitudes we used the data from Warner (2017b), with a rotation period of P = 7.52 h ± 0.01 and a composite light-curve amplitude of A = 0.38 mag, since it was obtained close to our observations, on 2017 March

8. Moreover, we corrected only the magnitudes obtained in dates close to the obtained light curve by Warner (2017b), the three points with smaller phase angles, since applying the correction to all points could generate a greater dispersion.

This NEO also has phase curve in the H-G_1–G_2 model determined by Mahlke, Carry & Denneau (2021), with phase angle coverage from 2.5° to 37.5° in the cyan filter, deriving an absolute magnitude and slope parameters of $H_{0c} = 14.96^{+0.08}_{-0.06}$, $G_1 = 0.0093^{+0.02}_{-0.009}$, and $G_2 = 0.6546^{+0.04}_{-0.04}$, and a phase angle coverage from 1.5° to 49.5° in the orange filter, deriving an absolute magnitude and slope parameters of $H_{0o} = 14.81^{+0.096}_{-0.08}$, $G_1 = 0.1281^{+0.07}_{-0.07}$, and $G_2 = 0.7384^{+0.04}_{-0.04}$. Both curves were derived with data from the Asteroid Terrestrial-impact Last Alert System telescope survey (ATLAS) catalogue (Tonry et al. 2021). Since the phase curve parameters are dependent on the used filter as well as on the phase angle coverage and to the removal or not of rotational effects, the above differences in the obtained values are to be expected.

3.1.2 (18109) 2000 NG11

The phase curve for this NEO belonging to the Amor group was obtained over 19 nights, between 2018 February and October, at OASI. It has the second best phase angle coverage, both in the OE region, with the lowest solar phase angle of 3.4°, and in the linear region, with data up to 34.8°. The phase curve is shown in Fig. 2 and the derived absolute magnitude and slope parameters are $H_{0R} =$

16.53, $G_1 = 0.8301$, and $G_2 = 0.01628$. It is noteworthy that due to the well covered phase curve, the fit has very small errors in the absolute magnitude, slope parameters, and fit.

The light curve used to correct for reduced magnitudes was determined by Monteiro et al. (2023) from observations obtained on 2018 November 11 and 12, at OASI. The derived rotational period has a value of P = 4.252 h $\pm$ 0.001 with a composite light-curve amplitude of $A = 0.84$ mag. Due to the large amplitude, corrections for rotational effects on the phase curve were applied only to the data obtained between November and December, corresponding to the phase angle interval of $27.3°$–$35°$. The remaining magnitudes were not corrected for rotation, a fact that might be responsible for the fluctuations visible around the fit at phase angles between 15 and 22. It is noteworthy, however, that this fact does not affect the determination of a very good fit to the data.

Finally it is important to mention that the rotational period of this NEO was previously determined by several authors (Pravec 2000; Warner 2014; Chang et al. 2015; Waszczak et al. 2015; Carbognani 2017; Warner & Stephens 2019), all with values similar to the one here determined, but none within the period of our observations. Moreover, it was taxonomically classified as C-type by Dandy et al. (2003) and as X-type by Carry et al. (2016), both from photometric spectra.

3.1.3 (65717) 1993 BX3

This asteroid, belonging to the Apollo group, has an albedo of $p_v = 0.15$ and a mean diameter of $D = 200$ m as given by Binzel et al. (2002), and it is the only PHA in our sample. For this object, it was possible to determine the colour V–R $= 0.484 \pm 0.309$, and from the equation (4), we derived an effective diameter of $D = 0.223 \pm 0.169$ km, similar to the Binzel et al. (2002) value. The phase curve was obtained at OASI over four nights between 2021 February 4 and March 13, with a phase angle coverage ranging from $7.9°$ up to $34.7°$.

The rotational period for this object was determined by diverse authors (Mottola et al. 1995; Pravec 2020; Warner & Stephens 2021) and we used the value obtained near our observations, between 2021 February and March, by Warner & Stephens (2021), i.e. P $= 20.331 \pm 0.002$ h and composite light-curve amplitude of $A = 0.83$ mag. As can be seen in Fig. 3, some points still show relatively large dispersion, which can be attributed to the individual error of each magnitude or/and the lack of data in the OE, besides the large range of phase angles, and the small amount of data which prevents a good fit. The derived values for the absolute magnitude and slope parameters are $H_{0R} = 20.45$, $G_1 = 0.9662$, and $G_2 = 0.0$.

3.1.4 (99799) 2002 LJ3

This NEO, of the Amor group, was observed at OASI from 2018 August to December. The derived values for the absolute magnitude and the slope parameters are $H_{0R} = 18.21$, $G_1 = 0.7792$, and $G_2 = 0.2208$, as shown in Fig. 4 and Table 2.

Although the phase curve is composed by data taken over several months, the correction for the rotational effects was performed using only one light curve determined by Monteiro et al. (2023) from observations on 2018 November 3, 5, 7, and 8 at OASI. These resulted in a rotational period of P $= 2.64 \pm 0.001$ h and amplitude of $A = 0.23$ mag. Due to the small light-curve amplitude, and the fact that the phase curve does not present large fluctuations, we believe that the performed corrections are reliable.
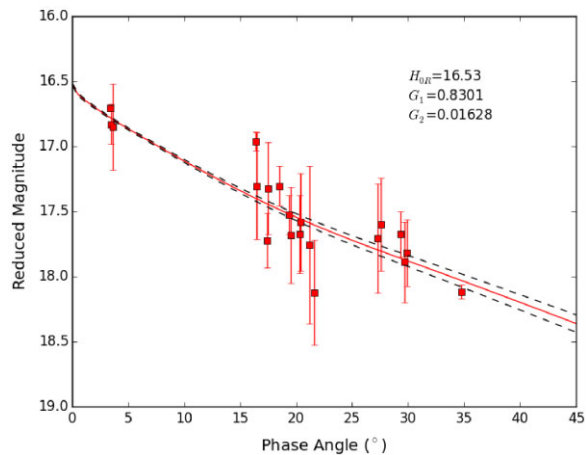

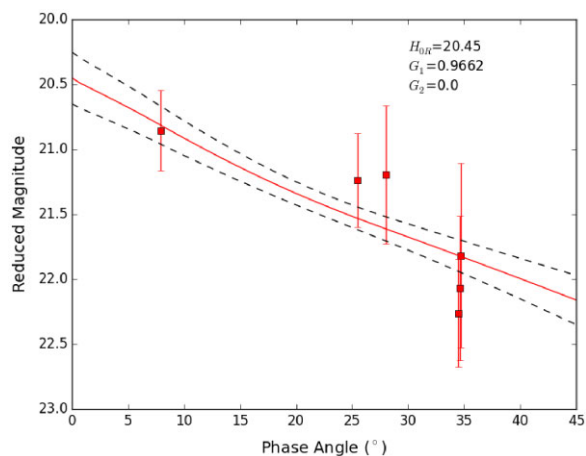**Figure 2.** Same as Fig. 1 for the NEO (18109) 2000 NG11.

Figure 3. Same as Fig. 1 for the NEO (65717) 1993 BX3.

This NEO has been observed by several authors resulting in slightly different taxonomic classifications such as Sq- by Thomas et al. (2014), S- by Carry et al. (2016), and Q-type by Binzel et al. (2019). Mueller et al. (2011), and Trilling et al. (2010) determined a high albedo of $p_v = 0.43$; however, our fit presents a flat behavior in the OE region which seems not to be compatible with such classification, according to Belskaya & Shevchenko (2000). Although, this can be due to the lack of data in the OE region, $\alpha < 5°$, in our phase curve. It is to be noted, however, that the good coverage in the linear region resulted in a small error in the fit.

3.1.5 (174050) 2002 CC19

This NEO is an object of the Amor group and was observed at OASI during five nights on 2021 February. The phase curve has a good coverage in the linear region, from $6.2°$ to $34.4°$ (Fig. 5), but lacking in the OE region. None the less, the fit indicate a significant opposition surge. Moreover, due to non-photometric conditions, the magnitudes present large errors which, in turn, lead to significant errors in the absolute magnitude and the slope parameters: $H_{0R} = 16.626$, $G_1 = 0.0$, and $G_2 = 0.1919$. With observations in the V-Johnson-Cousins filter, it was possible also to derive the colour V–R $= 0.230 \pm 0.472$.
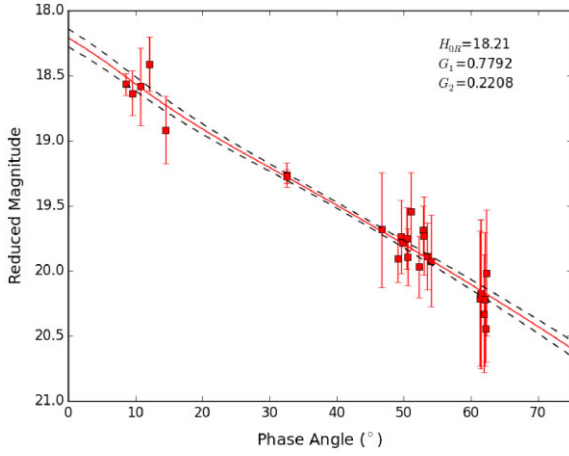
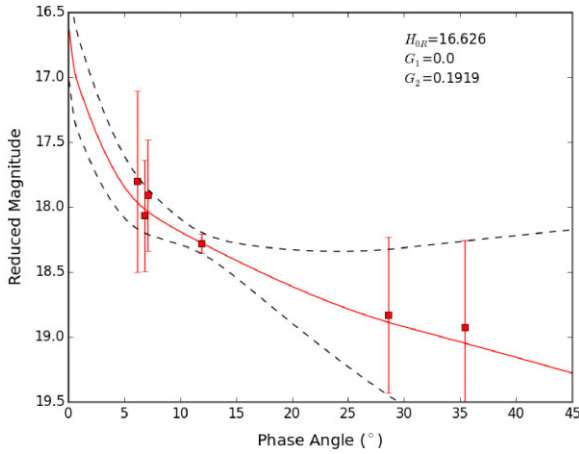**Figure 4.** Same as Fig. 1 for the NEO (99799) 2002 LJ3.

Figure 5. Same as Fig. 1 for the NEO (174050) 2002 CC19.

For this object, the light curve used to correct for the rotational effects was determined for us from observation at OASI on 2021 February 6 and 7. The data was fitted by a fourth-order Fourier series, giving a rotation period of 4.2344 ± 0.01 h and a composite light-curve amplitude of 0.181 mag. Using the quality code scheme developed by Harris & Young (1983), we attribute a quality code U = 2 to this composite light curve. The rotational light curve is shown in Fig. 6. A different values was derived by Pravec (2021), P = 3.514 ± 0.002 h and A = 0.086, from observations on 2021 February 12, 13, and 14, but also with a quality code U = 2 due to the low coverage of their data. The difference between the two rotational periods can be attributed to the poor data in both determinations, well represented by the assigned quality code of 2.

3.1.6 (175189) 2005 EC224

This target was observed over 16 nights, 12 between 2016 December and 2017 April, and 4 between 2020 May and June. A phase curve for this NEO in the H-G_1–G_2 model was previously obtained by Ieva et al. (2022), with a phase angle coverage from 0.7° to 29.3° and data obtained at CI. Including data obtained at OASI, we now reach a phase angle coverage from 0.7° up to 36.6°, resulting in the best OE coverage of our sample. Belonging to the Amor group, it has an albedo p_v = 0.204 and a diameter of D = 0.641 km determined by
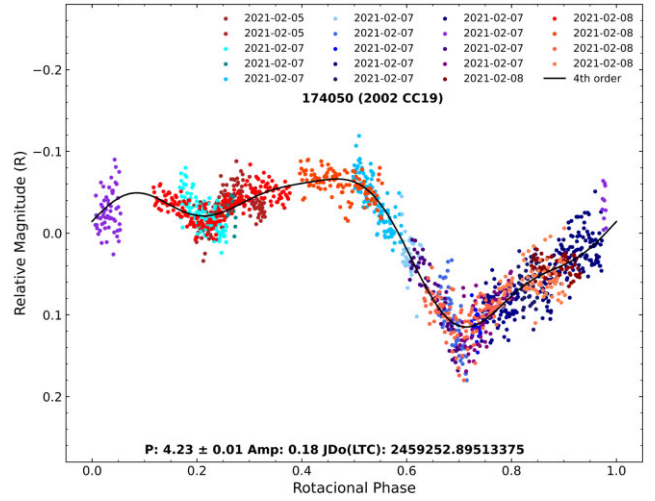

Figure 6. Composite light curve of the NEO (174050) 2002 CC19. The coloured dots are from February 5, 6, and 7, respectively. The black line indicate the best fit obtained with a fourth-order Fourier fit. The zero phase is on 2021/02/07 at 09:28:59 UT.
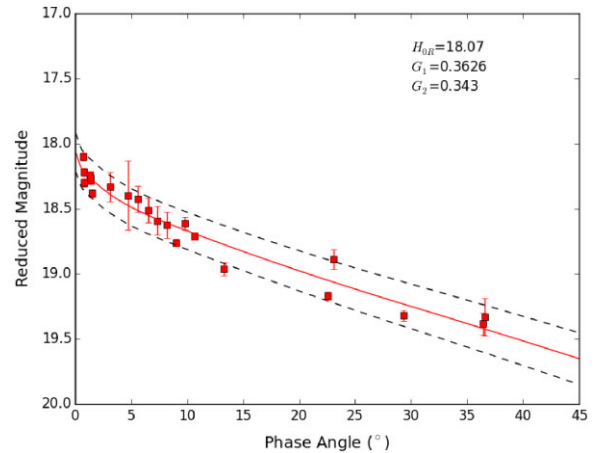

Figure 7. Same as Fig. 1 for the NEO (175189) 2005 EC224.

Masiero et al. (2020a). The derived values for the absolute magnitude and the slope parameters are H_{0R} = 18.07, G_1 = 0.3626, and G_2 = 0.343, as shown in Fig. 7.

For this object, it was not possible to correct the rotational effects, as we did not determined the rotation period and those given in the literature were not obtained at the same time of our data. However, according to Díaz-Vachier et al. (2022), Warner & Stephens (2020), and Pravec (2020), this object has a small rotational period amplitude, between 0.1 and 0.25 mag, which explains the non-fluctuation of the points on its phase curve. Anyhow, we have used the maximum amplitude of the rotational light curve to consider the uncertainty in the phase curve.

This NEO also has phase curve in the H-G_1–G_2 model determined by Mahlke et al. (2021), with a phase angle coverage from 0.69° to 52.29° in the orange filter, from data of the ATLAS catalogue, deriving an absolute magnitude and slope parameters of H_{0o} = $18.29^{+0.40}_{-0.40}$, G_1 = $0.580^{+0.67}_{-0.067}$ and G_2 = $0.377^{+0.026}_{-0.026}$. As mentioned above, the different filters and phase angle coverage might explain the differences in the derived parameters (see Section 4).
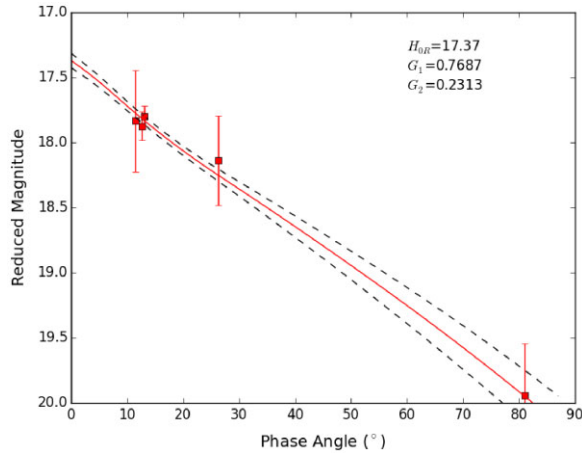
Figure 8. Same as Fig. 1 for the NEO (417581) 2006 VA3.

Figure 9. Same as Fig. 1 for the NEO (464797) 2004 FZ1.

Figure 10. Same as Fig. 1 for the NEO (480004) 2014 KD91.

3.1.7 (417581) 2006 VA3

Classified as an object of the Apollo group, this NEO has a determined albedo of $p_v = 0.145$ and a diameter of $D = 1.041$ km (Masiero et al. 2020b). This asteroid was observed at OASI over five nights between 2021 February and March, having the largest phase angle coverage of our sample: from $11.3°$ up to $81°$. Although the phase curve does not have a good coverage in the OE region, the fit presents very small errors. The phase curve is shown in Fig. 8 and the derived absolute magnitude and slope parameters are $H_{0R} = 17.37$, $G_1 = 0.7687$, and $G_2 = 0.2313$.

The light curve used to correct for rotational effects was determined by Monteiro et al. (2023), based on observations obtained on 2021 February 9, 10, 11, and 12, at the OASI. A period of P $= 5.481 \pm 0.002$ h and a composite light-curve amplitude of $A = 0.40$ mag were derived.

Lastly, we computed an effective diameter of $D = 0.959 \pm 0.283$ km, similar to the one derived by Masiero et al. (2020b), using equation (4), the absolute magnitude and albedo above, and the colour V–R $= 0.435 \pm 0.343$, derived here.

3.1.8 (464797) 2004 FZ1

This asteroid is classified as Sr-type by Binzel et al. (2019), with an albedo of 0.103 ± 0.060, and diameter $D = 0.975$ km determined by Masiero et al. (2020b). This target, belonging to the Apollo group, was observed during five nights in 2016 August, at OASI. The phase curve has an angle coverage from $8.8°$ to $17.4°$, and is shown in Fig. 9. Although the magnitudes that compose the phase curve have very small errors, which indicates that they were obtained on photometric nights, the absolute magnitude determined has significant errors. This is probably due to the non-coverage of the OE region and the small phase angle coverage, with points concentrated around $10°–25°$. The derived values for the absolute magnitude and slope parameters are $H_{0R} = 17.39$, $G_1 = 0.2593$, and $G_2 = 0.3831$.

This NEO has a rotational period of 45.4 ± 0.2 h with a composite light-curve amplitude of $A = 0.39$, determined by Warner (2017a) from data obtained over several nights on 2016 August. Thus, correction for rotational effects was performed using data from this light curve, acquired on the same period of our observations.
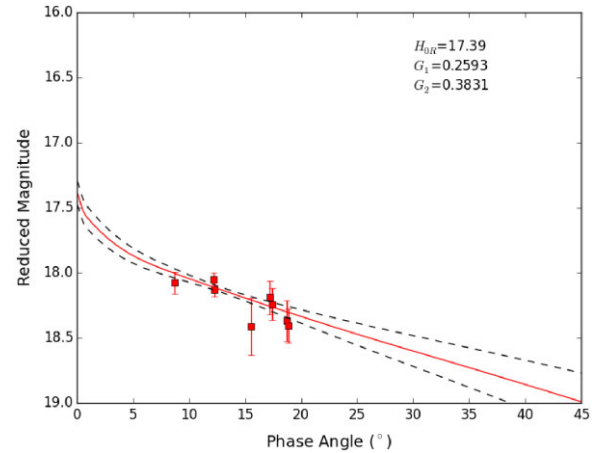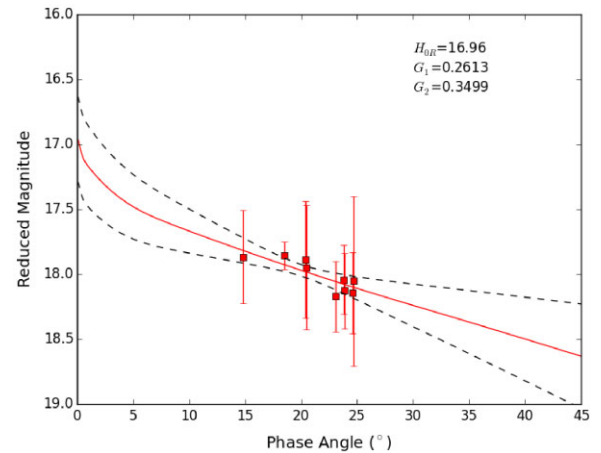
3.1.9 (480004) 2014 KD91

This asteroid of the Amor group, with a moderate albedo of 0.2 (Masiero et al. 2020a) and a diameter of 1.979 m (Masiero et al. 2020b), was observed at OASI during eight nights between 2016 September and October. This resulted in a small phase angle coverage, varying just from $14.8°$ to $26.6°$, and with no points in the OE region. Although a rotation period was previously determined by several authors (Warner 2016; Carbognani 2017; Vaduvescu et al. 2017; Monteiro et al. 2018) a new light curve was obtained in the same period of our observations. A period of 2.835 ± 0.001 h and a composite light-curve amplitude of $A = 0.17$ mag were determined (Monteiro et al. 2023).

The fitted phase curve, shown in Fig. 10, resulted in values for the absolute magnitude and slope parameters of $H_{0R} = 16.96$, $G_1 = 0.2613$, and $G_2 = 0.3499$. Due to the very concentrated data, and far from the OE region, the fit has large errors.

3.1.10 2011 YQ10

Classified as a NEO of the Amor group, this object was observed over seven nights between 2021 October and December. Its phase curve has a coverage from $5.9°$ up to $48.3°$ and shows a flat behavior in the region of the OE. It is to be noted that the phase angle coverage, although large, is very badly distributed, with just two
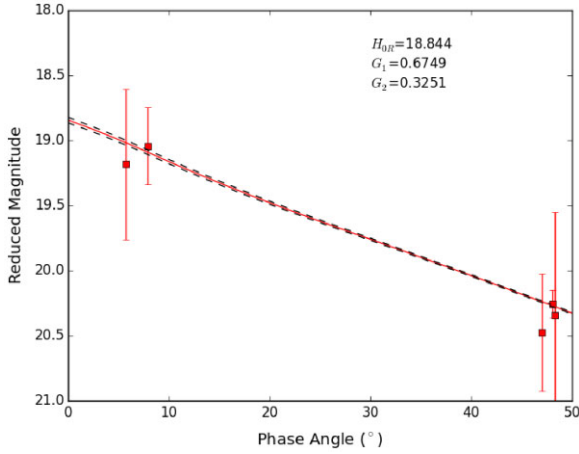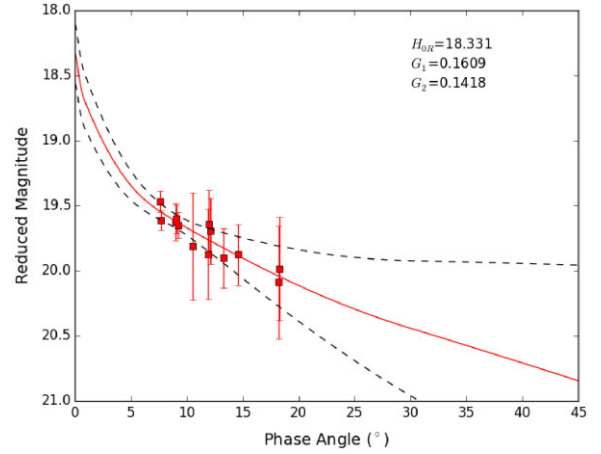
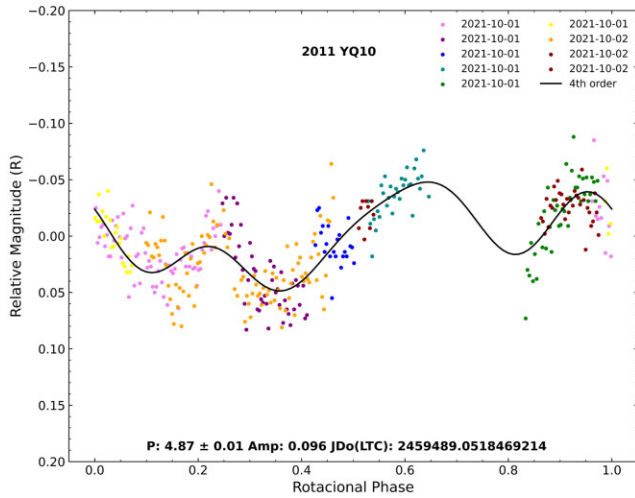**Figure 11.** Same as Fig. 1 for the NEO 2011 YQ10.

Figure 12. Composite light curve of the NEO 2011 YQ10. The green, coloured dots are from September 29 and 30 and October 1, respectively. The black line indicate the best fit obtained with a fourth-order Fourier fit. The zero phase is on 2021/10/01 at 13:14:40 UT.

small concentrations: one at about 6° and another at 48°. This lead to the small fit error beside the large errors in the reduced magnitudes. The fitted phase curve, shown in Fig. 11, provided values of the absolute magnitude and slope parameters of $H_{0R} = 18.844$, $G_1 = 0.6749$, and $G_2 = 0.3251$.

For this NEO, corrections for rotational effects were performed using a light curve obtained at OASI on 2021 September 29 and 30, and October 1 as shown in Fig. 12. The data was fitted by a fifth-order Fourier series, deriving a rotation period of P = 4.8651 ± 0.01 h and a composite light-curve amplitude of $A = 0.096$ mag, with a quality code U = 2. The period of this object was previously determined by other authors: a period of P = 4.824 ± 0.0007 h with a composite light-curve amplitude of $A = 0.08$ mag by Pravec (2021), and a period of P = 4.827 ± 0.002 h with a composite light-curve amplitude of $A = 0.14$ mag by Warner & Stephens (2022), with data obtained on 2021 November 8 and 2021 September 16, respectively. These values do not differ much from those determined here and although the light curve with the best coverage is the one determined by Warner & Stephens (2022), we used our data to perform the correction for rotational effects because it was obtained at the same

Figure 13. Same as Fig. 1 for the NEO 2016 RP33.
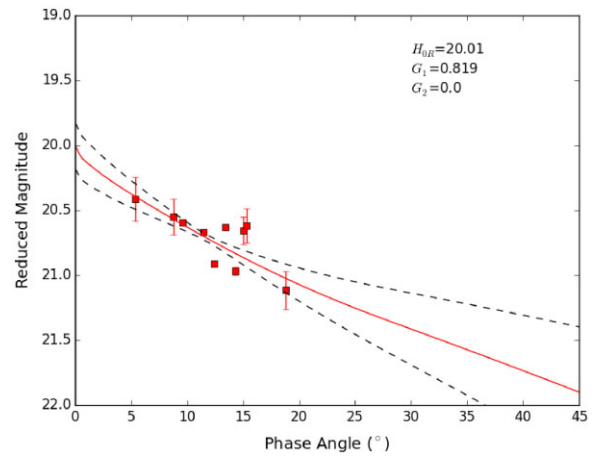
Figure 14. Same as Fig. 1 for the NEO 2017 AC5.

time as the phase curve. For this NEO we also derive the colour V–R = 0.496 ± 0.296.

3.1.11 2016 RP33

This NEO, belonging to the Amor group, was observed over seven nights on 2016 September. With a phase angle coverage from 7.6° to 14.7° (Fig. 13) and small coverage in the OE region, we have a good determination of the phase curve parameters with values of H_{0R} = 18.331 $G_1 = 0.1609$, and $G_2 = 0.1418$. It is to be noted that the significant opposition surge is based on just few points between 5° and 10°.

This object has a rotational period determined from observations on 2016 September both by Warner (2017a), P = 4.682 ± 0.002 h and $A = 0.15$ mag, and by Monteiro et al. (2018), P = 4.707 ± 0.001 h and $A = 0.22$ mag. The latter values were used since they were obtained on the same nights as our phase curve magnitudes.

3.1.12 2017 AC5

With data from 10 nights of observations between 2017 February and March, both at OASI and CI, we determined the phase curve shown in Fig. 14 for this NEO of the Amor group. This asteroid shows the smallest errors in magnitudes of all the sample, and the phase angle

coverage is from 5.4° to 18.8°. The absolute magnitude values and slope parameters of the curve are given by $H_{0R} = 20.01$, $G_1 = 0.819$, and $G_2 = 0.0$.

The rotational period of this NEO was determined by several authors (Erasmus et al. 2017; Vaduvescu et al. 2017; Warner 2017b; Pravec 2019; Ieva et al. 2020), but to correct our magnitudes we used the data from Warner (2017b) since it was obtained near our observations. The composite light curve reported by Warner (2017b) provided a rotational period of P = 5.922 ± 0.005 h and a high amplitude of $A = 0.81$ mag.

4 ANALYSIS

As already mentioned, important physical parameters of atmosphere-less bodies can be derived from their phase curve. However, it is important to consider that deriving physical properties of individual NEOs from their phase curves is not so simple since the often elongated shape of these objects and the significant variations in aspect angle during their appearances can cause additional variations in brightness on their phase curves (Kwiatkowski & Kryszczynska 1992; Jackson et al. 2022). The most direct being the absolute magnitude which, in turn, can lead to the determination of an object's effective diameter when its albedo is known. However, in our sample just seven objects, over 12, do have a published albedo beside the fact that our absolute magnitude is in the R filter when to compute the effective diameter (Lupton 2005), it should be in the V filter, for this reason we need also the colours V–R of the asteroid. Of course, it could be possible to infer the albedo of an object from its taxonomic classification. However, all these assumptions would tend to increases the associated errors in the computed effective diameter and we believe it will be sort of useless. In this way, we derived the diameter for only two of the four objects that we determined the V–R colour for, as they have a previously determined albedo.

On the other hand, the slope parameters G_1 and G_2 can help derive other physical properties such as high/low albedo and probable taxonomic class, when we are able to observe tendencies analysing large data sets. In Rondón et al. (2019), for example, was used the data from 93 MB with well-determined taxonomy and albedo, taken from the work by Shevchenko et al. (2016). Thus, a plot in the $G_1 \times G_2$ phase space allowed to see how the parameters derived for six NEOs fitted into the taxonomic type preferred regions defined in that work (see fig. 18 of Rondón et al. 2019). More recently was used a larger sample of 15 NEOs (Ieva et al. 2022) to derive their taxonomic classification using several techniques. Thus, we decided to use our now larger NEOs database, with the slope parameters for 30 NEOs, obtained mostly with the same instrumentation and with the same methodology (Rondón et al. 2019, 2022; Ieva et al. 2022; present work), to investigate their link to the MB population. But, in order to have robust results, we also need a larger database for the MB population than the one used in Shevchenko et al. (2016).

To this end, we used consider using the Asteroid Absolute Magnitude and Slope (AAMS) catalogue (Muinonen et al. 2010), (Oszkiewicz et al. 2011). This catalogue contains more than 46 000 MB objects with curve phase parameters in the H-G, H-G_{12}, and the H-G_1–G_2 models. However, when trying to reproduce Shevchenko et al. (2016) results regarding the G_1–G_2 phase space, using the same objects, we found great differences. This can be due to the larger errors in H in the AAMS catalogue as well as the fact that it does not specify in which filters the magnitudes were determined. When we tried to filter the sample using just objects with the smaller errors, the data set turns out to be too small to be useful.
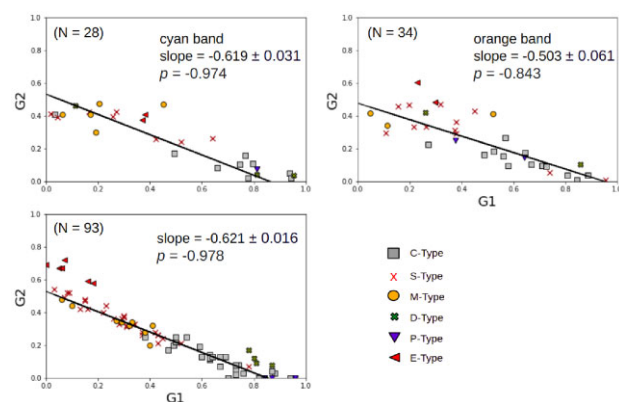

Figure 15. G_1 versus G_2 for a set of MB objects given in Shevchenko et al. (2016), lower panel, and for the same objects in the ATLAS catalogue in the cyan and orange filter, upper panels left and right, respectively. The different colours indicate the object's taxonomic classification as specified in the bottom right box, while the black line indicate the linear fits to the data with slope and standard deviation given in each figure.

Another recent catalogue of asteroid phase curves is from the ATLAS dual-band photometry[2] (Mahlke et al. 2021). This catalogue contains about 94 777 asteroid phase curves from dual-band photometry acquired by ATLAS (Tonry et al. 2018), with magnitudes observed in two filters: a passband between 420 and 650 nm called cyan and a pass-band between 560 and 820 nm called orange. Mahlke et al. (2021) using this catalogue gives phase curve parameters in the H-G_{12} and the H-G_1–G_2 models, although we used just the last one since it is the same used in our works. The phase angle coverage and standard deviation of H-G_1–G_2 model fit are also given in catalogue, which will be shown below that it is more in accordance with the Shevchenko et al. (2016) results.

In what follows we will first analyse the correlation between G_1–G_2 and the albedo for the MB population, as in the work by Shevchenko et al. (2016), then we will analyse the same correlation with the diameter, and, finally, discuss how our NEOs fit into this scenario.

4.1 Correlation G_1–G_2 for the MB

As a first step, we searched for the 93 Shevchenko et al. (2016) objects in the phase curves in the ATLAS dual-band photometry and found 28 objects with curves in the cyan band and 34 in the orange band. Fig. 15 shows the correlation between G_1 and G_2 for the ATLAS data (upper panels) and from Shevchenko et al. (2016; bottom panel) for comparison. The different point colours represent the different taxonomic classification of the asteroids while the black line is the linear fit, which was computed not considering the D- and E-type objects, as in Shevchenko et al. (2016). The bottom panel shows clearly the separation of the S- and M-type objects in the upper left region of the fit and the C- and P-type in the bottom right region. In the case of the data from ATLAS observations, the data appears more scattered, probably due to the smaller number of objects, but, generally it reproduces well the Shevchenko et al. (2016) results.

It is noteworthy that Mahlke et al. (2021) finds evidence of wavelength dependence of phase curve coefficients; this dependence is also observed with the change of the linear fit slope with the filter used (Fig. 15, upper left- and right-hand panel). Analysing the cyan
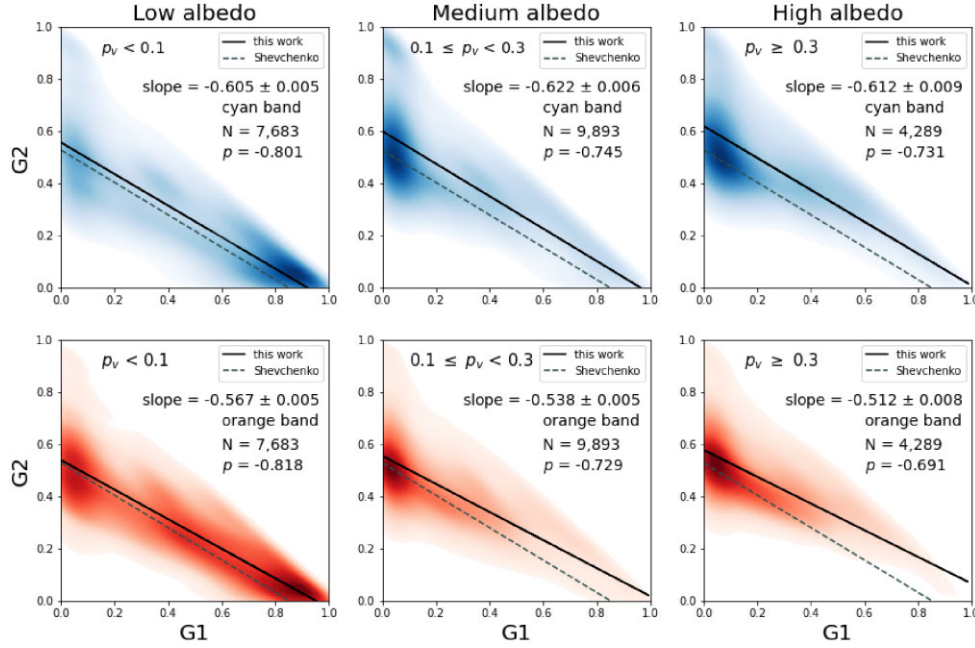
[2]https://vizier.cds.unistra.fr/viz-bin/VizieR?-source=VII/288

Figure 16. G_1, G_2-distributions for three albedo ranges: low albedo, medium albedo, and high albedo, comprising 21 865 objects, from asteroid phase curves catalogue from ATLAS dual-band photometry, observed in cyan (blue fit) and orange (red fit). The distributions are represented by 2D Gaussian kernel density estimators (KDE) fitted to the G_1, G_2-pairs. The black line corresponds to the linear fit of the sample with slop value shown, and the dashed line corresponds to the linear fit with the 93 MB of the Shevchenko et al. (2016) work, for comparison. N is the number of asteroids in each albedo range, and p is the Pearson correlation coefficient. (For interpretation of the references to colour in this figure legend, the reader is referred to the web version of this article.).

and orange filters used by ATLAS Survey (Tonry et al. 2018), and the V and R filters of Johnson-Cousins system, we found that the passband of the V filter, between 470 and 700 nm, is similar to that of the cyan band, while the passband of the R filter, between 550 and 900 nm, is similar to the orange band. This may explain the similarity of the slope of the linear fit of the data obtained in the cyan band, of -0.619, with that from the Shevchenko et al. (2016) data, of -0.621, where most of the objects were obtained in the V filter of the Johnson-Cousin system (Fig. 15, left upper and left lower panel). Using the Pearson correlation coefficient, we also observe a strong correlation between the parameters G_1 and G_2, of -0.974 and of -0.978, for the cyan band and Shevchenko et al. (2016) data, respectively. Again it is important to note the similarity between the two values.

As the distribution in G_1–G_2 phase space is related to the wavelength, as shown by Mahlke et al. (2021), as a second step, we used phase curves from the ATLAS catalogue that have data in both the cyan and orange bands. Of these objects, we used only those with an albedo determined by NEOWISE (Mainzer et al. 2011), obtaining a sample of 21 865 MB objects.

In Fig. 16, we give the G_1, G_2-distributions for three albedo ranges: low albedo, medium albedo, and high albedo, comprising 21 865 objects, from asteroid phase curves catalogue from ATLAS dual-band photometry, observed in cyan (blue fit) and orange (red fit). The distributions are represented by 2 D Gaussian kernel density estimators (KDE; Waskom et al. 2020), of the seaborn package from python, fitted to the G_1, G_2-pairs. These intervals were defined as low $p_v < 0.1$, medium $0.1 \leq p_v < 0.3$ and high $p_v \geq 0.3$. The black line corresponds to the linear fit of the sample and the dashed line to the linear fit to 93 MB from Shevchenko et al. (2016), just for comparison. We can see that the clustering is similar in both band; however, in the low albedo range in the orange filter we

observe a second cluster with less density. On the other hand, for low albedo we observe that the clustering is in lower-right, while in the medium and high albedo is in upper-left, this clearly show a dependence of the parameters G_1–G_2 with the albedo. However, analysing individual objects is not enough to derive the albedo. Lastly, we observe that the correlation between the parameters remains as well as a dependence of the linear fit slope with the filters with values about -0.6 and -0.5 for the cyan and orange band, respectively.

The albedo-dependence of the OE and photometric slope described by Belskaya & Shevchenko (2000) has been extensively explored to study the correlation between the taxonomy of an asteroid and the slope parameters of the phase curve G_1–G_2 (Penttilä et al. 2016; Shevchenko et al. 2016; Rondón et al. 2019; Ieva et al. (2022). However, the question is whether the object's size has any influence on this correlation.

To better analyse this point, we used KDE 2 D adjusted to the G_1–G_2 parameter for three diameter ranges: $D < 10$ km, 10 km $< D < 50$ km, and $D > 50$ km. The result is shown in Fig. 17 where the black and dashed lines are as in Fig. 16. We observe that the clustering is similar in both band. For $D < 10$ km we observe that the clustering is in upper-left, while for $D > 10$ km it is in lower-right, which clearly show a dependence of the parameters G_1, G_2 with the size. We also observe a dependence of the linear fit slope with the filter and the size.

We further analysed this point repeating the KDE 2 D to the parameters G_1–G_2 for the three diameter ranges and each albedo range. The results are shown in Figs 18, 19, and 20 for the low, medium and high albedo, respectively. These figures clearly show the strong dependence of the G_1 and G_2 phase space with the objects size. When separating by albedo and diameter, we see that the position of the concentration of objects is independent of the filter and that
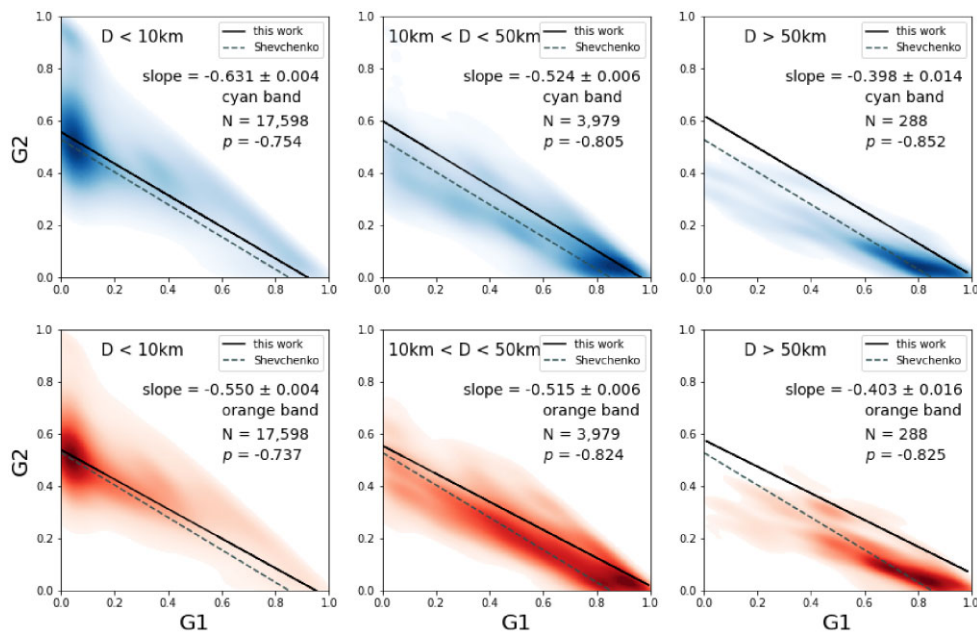
Figure 17. Distribution of G_1, G_2 for three diameter range $D < 10$ km, 10 km $< D < 50$ km, and $D < 50$ km.
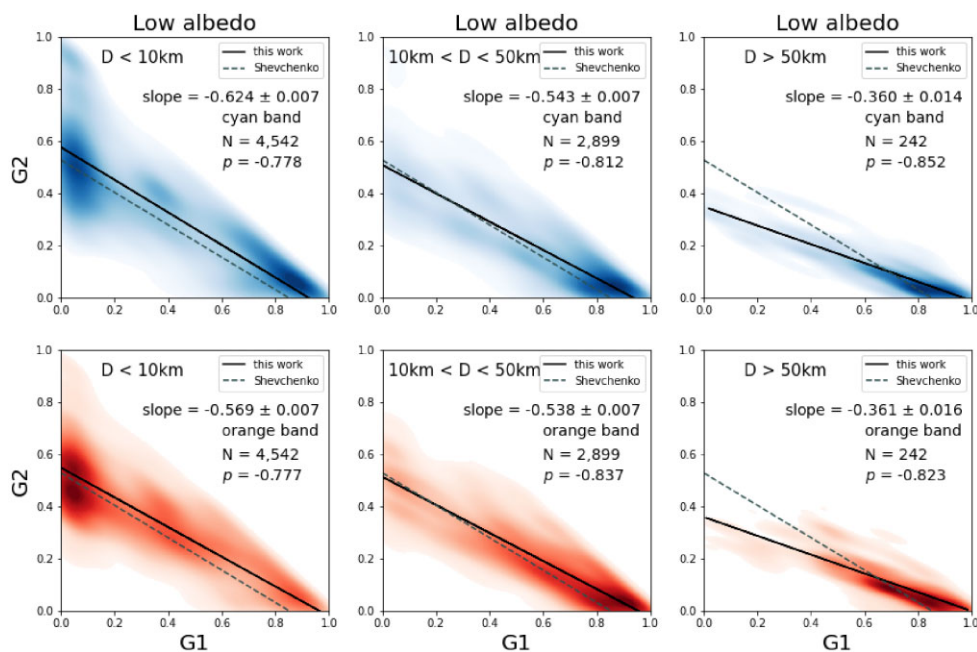

Figure 18. Similar to Fig. 18. but separating by diameters the objects with low albedo classification, with a sample of 7683 objects.

for objects with $D > 10$ km the behavior is very similar to that already found by Shevchenko et al. (2016), with low albedo objects in the lower-right region, medium albedo in the central part, and high albedo in the upper-left. On the other hand, objects with $D < 10$ km are always concentrated in the upper-left region of the correlation, regardless of the albedo. Finally, we see that the correlation slope, for each albedo range in both filters, decreases as the size of the asteroid diameter increases.

Regarding the slope this also differs depending on the objects size, independently of the band. Lets consider the blue band. For the small low albedo objects the slope is around -0.64, but it decreases as the sizes increases, up to -0.36 for objects with $D > 50$ km. The same

occurs, to a lesser extent, for medium and high albedo objects, going from -0.62 to -0.41, and from -0.61 to -0.48, respectively.

These analysis highlights the surprising result that the G_1 *vs* G_2 phase space has strong dependence on the size as well as the albedo of the objects. Therefore, having the position of an object in this space does not necessarily indicates its albedo, which depends also on the object size.

4.2 NEOs versus MB

Having obtained the general distribution of MB objects in the G_1 *vs* G_2 phase space according to their albedo and size, we will now
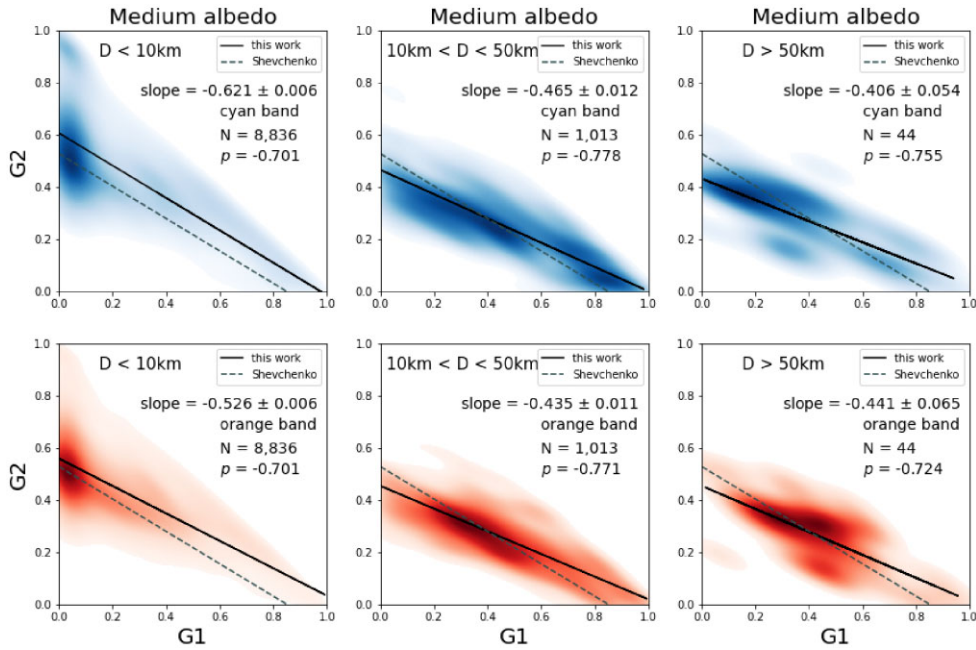
Figure 19. Similar to Fig. 18. but separating by diameters the objects with medium albedo classification, with a sample of 9893 objects.
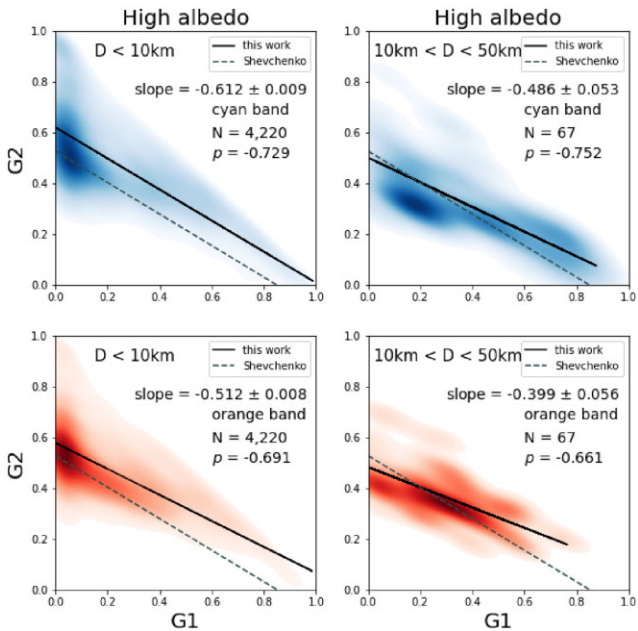

Figure 20. Similar to Fig. 18. but separating by diameters the objects with medium albedo classification, with a sample of 4289 objects.

turn to our NEOs and see what information can be obtained. The data set include phase curve parameter for 30 NEOs obtained in the present work as well as by Rondón et al. (2019, 2022), and by Ieva et al. (2022), including just one determination for each object (for convenience, the complete list is given in Table A2). As mentioned above, this set is quite homogeneous since all the phase curve parameters were obtained using the same procedures. We also found 73 NEOs in the database of phase curves obtained with ATLAS observations and in the orange band. Including these objects to our 30 NEOs that have phase curves determined in the R filter of the Johson-Cousins system, we obtained a sample of 103

NEOs. Considering that NEOs are all small, with diameter smaller than 10 km, and that our phase curve were determined in the R filter of the Johnson-Cousins system, more similar to the ALTAS orange band, in Fig. 21 we compared only the G_1, G_2 of MB for this size and band for three albedo ranges – low, medium, and high – (as given in Figs 18, 19, and 20) with the NEOs sample. The NEOs from this work, from Rondón et al. (2019, 2022), and from Ieva et al. (2022) are indicated by red symbols, while those from Mahlke et al. (2021) in green, purple, yellow, and grey. The black line correspond to the linear fit of the MB sample, as given in Figs 18, 19, and 20.

Analysing Fig. 21 upper panels, we clearly notice that most of the NEOs follow a correlation, as in the case of the MB objects. It can be noted that some NEOs present large dispersion from the fit, due to the large error in the phase curve, to be attributed in some cases to the lack of correction for rotational effects as for asteroids (16816) 1997 UF9 and (159608) 2002 AC2, or to large errors in the magnitudes, as for (174 050) 2002 CC19, (489 337) 2006 UM and 2005 TF. Accounting for the rotational effects and having a good phase angle coverage allows us to have more accurate G_1 and G_2 values. In the case of the (326 683) 2002 WP, for example, a first phase curve was obtained in Rondón et al. (2019), and the object showed a great dispersion from the linear fit (see fig. 18 in Rondón et al. 2019). However, after a better coverage of the phase angle, obtained in Ieva et al. (2022), the same object shows a smaller dispersion from the linear trend.

Investigating the slope parameters of all the sample of 103 NEOs, a linear fit slope of -0.521 ± 0.044 was obtained (Fig. 21 bottom panel). We also observed a strong linear correlation between parameters G_1 and G_2, with a correlation coefficient of -0.758. This strong correlation was also observed by Muinonen et al. (2010) and Shevchenko et al. (2016), but in our case we cannot use this correlation to infer the albedo since the distribution does not show any clear preference region with the albedo, which can also be caused by the significant error associated with the data. Therefore, data with more precise parameters are needed to have a good understanding of the behavior of small bodies in the phase space G_1 vs G_2.
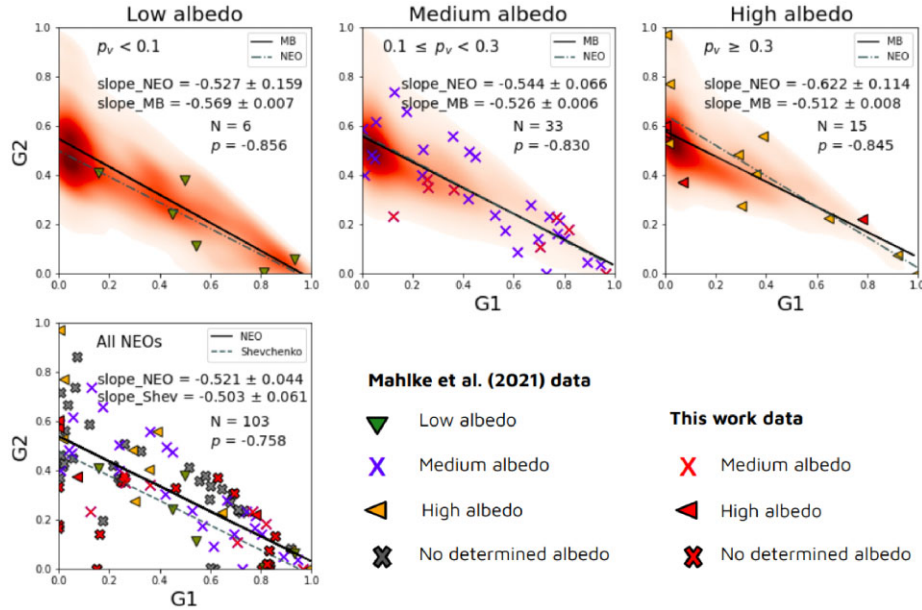
Figure 21. Same as Fig. 16 for distributions by 2D Gaussian KDE fitted to the G_1, G_2-pairs for MB $D < 10$ km with three albedo ranges for all NEOs with determined albedo (upper panels), and for all 103 NEO sample (bottom panel). The different symbols indicate the object's albedo classification as specified in the bottom right box, while the black line indicate the linear fits to the MB data and dashed line indicate the linear fits to the NEO. The red symbols represent data from the present work, from Rondón et al. (2019, 2022), and from Ieva et al. (2022) while other colours represent data from Mahlke et al. (2021).

As can be seen in Fig. 21, the values of the slope parameters between NEOs and MB with sizes smaller than 10 km is very similar, reflecting the likeness of the R and orange bands. On the other hand, no specific concentrations are observed among NEOs in the G_1–G_2 phase space, which can be attributed to the small sample. Moreover, as can be observed in the size distribution shown in Fig. 22, the NEOs are much smaller than the MB objects, even the smallest ones, and in order to compare the two samples we need to have comparable sizes in both samples.

5 CONCLUSIONS

In the present study we have determined the phase curves, corrected for rotational effects for twelve NEOs, nine belonging to the Amor group and three to the Apollo group, with one classified as PHA. This is a substantial addition to the available NEO data set for which the phase angle coverage has been well measured, in most cases in the OE region and in the linear part of the phase curve.

In order to perform the correction for rotational effects we also obtained light curves for most of the NEOs with complementary observations over the same period as the phase curve magnitudes. New values for the rotation periods of two NEOs – (174050) 2002 CC19 and 2011 YQ10 – are here presented while the rest will be described in Monteiro et al. (2023).

In the search for correlations between the G_1 and G_2 parameters, which could indicate physical properties of the studied objects, we analysed the behaviour of a large sample of MB asteroids phase curves from dual-band photometry (Mahlke et al. 2021) acquired by ATLAS (Tonry et al. 2018). This catalogue contains phase curves with magnitudes observed in two filters, called cyan and orange. When comparing the G_1 and G_2 correlations between the orange and cyan filters of the ATLAS survey, for the objects shown by Shevchenko et al. (2016), we see that the slopes are different (Fig. 15), which indicates that the parameters G_1 and G_2 are dependent on the used filters. On the other hand, we see that the correlation of G_1 vs G_2 shown by Shevchenko et al. (2016) with data that were acquired

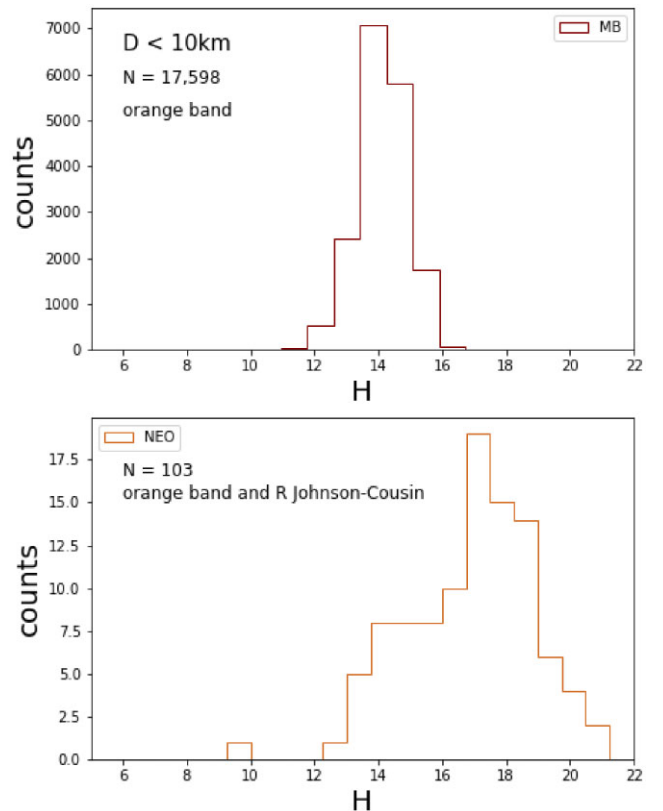**Figure 22.** Histogram of the absolute magnitude of MB with $D < 10$ km (upper panel), and of our sample of NEOs (lower panel).

in the Johnson V filter is similar to the correlation in the cyan filter of the ATLAS survey (Fig. 15; upper left and lower left), while the G_1 vs G_2 correlation of our NEOs, which were observed in the R-Cousins filter (Fig. 21; lower panel) is similar to the correlation in the

ATLAS orange filter (Fig. 15; upper right). This was to be expected, because the passband and the effective wavelength of the cyan and orange filter is very close to the filters V and R of the Johnson-Cousin system, respectively, and as we know the G_1 and G_2 values depend of the filter.

When analysing the phase space G_1 vs G_2 for MB objects we found that there is a strong correlation not only on the albedo, but also on the size. For asteroids with D>10 Km the behavior is similar to that shown by Shevchenko et al. (2016) while for those with $D <$ 10 km there is just one preferred region in the phase space G_1 vs G_2. It is important to note that the size was not considered in previous analysis [see for example Shevchenko et al. (2016)] and this is the first time that it has been proven to be an important parameter.

Finally, when we studying the behavior of the NEOs in the G_1 vs G_2 phase space and compare with that of the MB we observe that the slope of NEOs is similar to the MB with diameter less than 10 km. On the other side, we note that no preferential region is visible in the G_1 vs G_2 space depending on the albedo. This makes it difficult to infer a NEO albedo just for its position in the G_1 vs G_2 space. More observations are clearly necessary to understand the behaviors here described.

Last, but not least, in this work we show once more the importance of a dedicated telescope, such as OASI, as well as coordinated efforts, in order to achieve a good determination of important physical properties of NEOs, especially when continuous observations are of upmost importance, such as in the case of phase curves.

ACKNOWLEDGEMENTS

DATA AVAILABILITY

The data underlying this study are available in the article.

REFERENCES

Belskaya I. N., Shevchenko V. G., 2000, Icarus, 147, 94
Binzel R. P., Lupishko D., di Martino M., Whiteley R. J., Hahn G. J., 2002, in, Asteroids III. Univ. Arizona Press, Tucson, p. 255
Binzel R. P., Reddy V., Dunn T. L., 2015, in, Asteroids IV. Univ. Arizona Press, Tucson, p. 243
Binzel R. P. et al., 2019, Icarus, 324, 41
Bottke W. F., Morbidelli A., Jedicke R., Petit J.-M., Levison H. F., Michel P., Metcalfe T. S., 2002, Icarus, 156, 399
Carbognani A., 2017, Minor Planet Bull., 44, 52
Carry B., Solano E., Eggl S., DeMeo F. E., 2016, Icarus, 268, 340
Chang C.-K. et al., 2015, ApJ, 150, 27
Dandy C. L., Fitzsimmons A., Collander-Brown S. J., 2003, Icarus, 163, 363
Díaz-Vachier I., Cotto-Figueroa D., Rivas-Díaz A., Abreu-Cintrón J., Rivera-Rivera B., Santana-Rodriguez P., Laureno-La Puerta F., 2022, Minor Planet Bull., 49, 14
Erasmus N., Mommert M., Trilling D. E., Sickafoose A. A., van Gend C., Hora J. L., 2017, AJ, 154, 162
Hapke B., 1981, J. Geophys. Res., 86, 4571
Hapke B., 1984, Icarus, 59, 41
Hapke B., 1986, Icarus, 67, 264
Harris A. W., Lagerros J. S. V., 2002, in, Asteroids III. Univ. Arizona Press, Tucson, p. 205
Harris A. W., Young J. W., 1983, Icarus, 54, 59
Harris A. W. et al., 1989, Icarus, 77, 171
Helfenstein P., Veverka J., 1989, in Binzel R. P., Gehrels T., Matthews M. S.eds, Asteroids II. Univ. Arizona Press, Tucson, p. 557
Howell S. B., 1989, PASP, 101, 616
Ieva S. et al., 2020, A&A, 644, A23
Ieva S. et al., 2022, MNRAS
Irvine W. M., 1966, J.Geophys. Res., 71, 2931
Jackson S. L., Rozitis B., Dover L. R., Green S. F., Kolb U. C., Andrews A. E., Lowry S. C., 2022, MNRAS, 513, 3076
Kwiatkowski T., Kryszczynska A., 1992, in Brahic A., Gerard J. C., Surdej J.eds, Liege International Astrophysical Colloquia Vol. 30. Institut d'Astrophysique, Liege, p. 353
Landolt A. U., 1992, AJ, 104, 340
Lazzaro D., 2010, Bol. Asociacion Argentina de Astronomia La Plata Argentina, 53, 315
Lin C.-H., Ip W.-H., Lin Z.-Y., Cheng Y.-C., Lin H.-W., Chang C.-K., 2018, Planet. Space Sci., 152, 116
Lumme K., Bowell E., 1981, AJ, 86, 1705
Lupton, 2005, Transformations Between SDSS Magnitudes and UBVRcIc, http://www.sdss3.org/dr8/algorithms/sdssUBVRITransform.php (accessed April 2023)
Mahlke M., Carry B., Denneau L., 2021, Icarus, 354, 114094
Mainzer A. et al., 2011, ApJ, 731, 53
Masiero J. R. et al., 2020a, The Planetary Science Journal, 1, 5
Masiero J. R., Smith P., Teodoro L. D., Mainzer A. K., Cutri R. M., Grav T., Wright E. L., 2020b, The Planetary Science Journal, 1, 9
Michel P., Zappalà V., Cellino A., Tanga P., 2000, Icarus, 143, 421
Mishchenko M. I., 1992, Ap&SS, 194, 327
Mishchenko M. I., Dlugach Z. M., 1992, Ap&SS, 189, 151
Mishchenko M. I., Dlugach J. M., Liu L., Rosenbush V. K., Kiselev N. N., Shkuratov Y. G., 2009, ApJ, 705, L118
Monteiro F., Arcoverde P., Medeiros H., Rondon E., Souza R., Rodrigues T., Lazzaro D., 2018, Minor Planet Bull., 45, 221
Monteiro F. et al., 2023, Icarus, 390, 115297
Morbidelli A., Walsh K. J., O'Brien D. P., Minton D. A., Bottke W. F., 2015, in Michel P., DeMeo F. E., Bottke W. F.eds,, Asteroids IV. Univ. Arizona Press, Tucson, p. 493
Morozhenko A. V., Vidmachenko A. P., 2013, Kinematics Phys. Celestial Bodies, 29, 228
Mottola S., De Angelis G., Di Martino M., Erikson A., Hahn G., Neukum G., 1995, Icarus, 117, 62
Mueller M. et al., 2011, AJ, 141, 109
Muinonen K., Belskaya I. N., Cellino A., Delbò M., Levasseur-Regourd A.-C., Penttilä A., Tedesco E. F., 2010, Icarus, 209, 542
Muinonen K., Mishchenko M. I., Dlugach J. M., Zubko E., Penttilä A., Videen G., 2012, ApJ, 760, 118
Oszkiewicz D. A., Bowell E., Trilling D., Penttilä A., Pienluoma T., Wasserman L. H., Enga M. T., 2011, J. Quant. Spectrosc. Radiat. Transfer, 112, 1919
Penttilä A., Shevchenko V. G., Wilkman O., Muinonen K., 2016, Planet. Space Sci., 123, 117
Pravec, 2000, 'Prepublished' Periods of Asteroids, https://www.asu.cas.cz/ pravec/newres.htm (accessed April 2023)
Pravec, 2019, 'Prepublished' Periods of Asteroids, https://www.asu.cas.cz/ pravec/newres.htm (accessed April 2023)

Pravec, 2020, 'Prepublished' Periods of Asteroids, https://www.asu.cas.cz/ p pravec/newres.htm (accessed April 2023)

Pravec, 2021, 'Prepublished' Periods of Asteroids, https://www.asu.cas.cz/ p pravec/newres.htm (accessed April 2023)

Rondón E., Arcoverde P., Monteiro F., Medeiros H., Navas G., Lazzaro D., Carvano J. M., Rodrigues T., 2019, MNRAS, 484, 2499

Rondón E. et al., 2020, PASP, 132, 065001

Rondón E. et al., 2022, Icarus, 372, 114723

Sanchez J. A., Reddy V., Nathues A., Cloutis E. A., Mann P., Hiesinger H., 2012, Icarus, 220, 36

Sanchez J. A., Michelsen R., Reddy V., Nathues A., 2013, Icarus, 225, 131

Shevchenko V. G. et al., 2016, Planet. Space Sci., 123, 101

Shkuratov Y. G., Kreslavsky M., Ovcharenko A., Stankevich D., Zubko E., Pieters C., Arnold G., 1999, Icarus, 141, 132

Tedesco E. F., Veeder G. J., Fowler J. W., Chillemi J. R., 1992, The IRAS Minor Planet Survey. Philliips Laboratory, Hanscom Air Force Base, MA

Thomas C. A., Emery J. P., Trilling D. E., Delbó M., Hora J. L., Mueller M., 2014, Icarus, 228, 217

Tonry J. L. et al., 2018, Astronomical Society of the Pacific, 130, 064505

Tonry J. L. et al., 2021, VizieR Online Data Catalog, p. J/ApJ/867/105

Trilling D. E. et al., 2010, AJ, 140, 770

Vaduvescu O. et al., 2017, Earth Moon Planets, 120, 41

Vereš P. et al., 2015, Icarus, 261, 34

Warner B. D., 2014, Minor Planet Bull., 41, 113

Warner B. D., 2016, Minor Planet Bull., 43, 66

Warner B. D., 2017a, Minor Planet Bull., 44, 22

Warner B. D., 2017b, Minor Planet Bull., 44, 223

Warner B. D., 2019, MPO Softwere, MPO Canopus v10.8.1.1., http://minorplanetobserver.com (accessed April 2023)

Warner B. D., Stephens R. D., 2019, Minor Planet Bull., 46, 27

Warner B. D., Stephens R. D., 2020, Minor Planet Bull., 47, 290

Warner B. D., Stephens R. D., 2021, Minor Planet Bull., 48, 294

Warner B. D., Stephens R. D., 2022, Minor Planet Bull., 49, 16

Warner B. D., Harris A. W., Pravec P., 2009, Icarus, 202, 134

Waskom M. et al., 2020, mwaskom/seaborn: v0.11.1 (December 2020), Zenodo, available at: https://zenodo.org/record/4379347

Waszczak A. et al., 2015, AJ, 150, 75

Zappala V., Cellino A., Barucci A. M., Fulchignoni M., Lupishko D. F., 1990, A&A, 231, 548

APPENDIX A: ADDITIONAL TABLES

In the following tables for each asteroid are given the reduced magnitudes corrected by rotational period and the derived H-G_1–G_2 values.

Table A1. Derived magnitudes.

Asteroid	Observatory	Date	mag	α (°)
(4055) Magellan	CI	2017/03/12	14.333 ± 0.063	3.0
	CI	2017/03/01	14.639 ± 0.027	4.0
	CI	2017/02/27	14.649 ± 0.027	5.0
	CI	2017/03/17	14.722 ± 0.027	5.8
	CI	2017/02/20	14.899 ± 0.027	8.9
	CI	2017/03/24	14.839 ± 0.021	10.0
	CI	2017/03/28	14.889 ± 0.021	12.2
	CI	2017/03/31	15.019 ± 0.027	13.7
(18109) 2000 NG11	OASI	2018/09/06	16.707 ± 0.007	3.4
	OASI	2018/09/09	16.829 ± 0.151	3.5
	OASI	2018/09/05	16.848 ± 0.331	3.6
	OASI	2018/08/12	16.960 ± 0.074	16.4
	OASI	2018/10/03	17.304 ± 0.410	16.5
	OASI	2018/08/10	17.723 ± 0.211	17.4
	OASI	2018/10/05	17.322 ± 0.356	17.5
	OASI	2018/10/07	17.304 ± 0.151	18.5
	OASI	2018/08/06	17.524 ± 0.152	19.4
	OASI	2018/10/09	17.681 ± 0.368	19.5
	OASI	2018/10/11	17.674 ± 0.301	20.3
	OASI	2018/10/11	17.581 ± 0.377	20.4
	OASI	2018/10/13	17.754 ± 0.607	21.2
	OASI	2018/10/14	18.122 ± 0.405	21.6
	OASI	2018/10/31	17.706 ± 0.419	27.3
	OASI	2018/11/01	17.602 ± 0.356	27.6
	OASI	2018/11/08	17.676 ± 0.174	29.3
	OASI	2018/11/10	17.889 ± 0.310	29.7
	OASI	2018/11/11	17.820 ± 0.255	29.9
	OASI	2018/12/11	18.117 ± 0.052	34.8
(65717) 1993 BX3	OASI	2021/03/13	20.854 ± 0.309	7.9
	OASI	2021/02/11	21.235 ± 0.362	25.5
	OASI	2021/02/09	21.195 ± 0.533	28.0
	OASI	2021/02/04	22.260 ± 0.414	34.5
	OASI	2021/02/04	22.068 ± 0.559	34.6
	OASI	2021/02/04	21.816 ± 0.712	34.7
(99799) 2002 LJ3	OASI	2018/09/06	18.565 ± 0.086	8.6
	OASI	2018/09/09	18.636 ± 0.173	9.6
	OASI	2018/09/05	18.584 ± 0.298	10.8
	OASI	2018/08/12	18.410 ± 0.211	12.1
	OASI	2018/10/03	18.917 ± 0.260	14.5
	OASI	2018/08/10	19.261 ± 0.095	32.5
	OASI	2018/10/05	19.272 ± 0.052	32.6
	OASI	2018/10/07	19.684 ± 0.441	46.7
	OASI	2018/08/06	19.904 ± 0.182	49.1
	OASI	2018/10/09	19.739 ± 0.281	49.6
	OASI	2018/10/11	19.779 ± 0.034	49.8
	OASI	2018/10/11	19.752 ± 0.238	50.4
	OASI	2018/10/13	19.896 ± 0.219	50.6
	OASI	2018/10/14	19.541 ± 0.296	51.1
	OASI	2018/10/31	19.968 ± 0.237	52.3
	OASI	2018/11/01	19.690 ± 0.193	52.9
	OASI	2018/11/08	19.731 ± 0.299	53.0
	OASI	2018/11/10	19.889 ± 0.256	53.5
	OASI	2018/11/11	19.923 ± 0.354	54.1
	OASI	2018/12/11	20.211 ± 0.519	61.3
	OASI	2018/11/01	20.178 ± 0.571	61.5
	OASI	2018/11/08	20.329 ± 0.454	61.9
	OASI	2018/11/10	20.221 ± 0.513	62.1
	OASI	2018/11/11	20.443 ± 0.260	62.2
	OASI	2018/12/11	20.017 ± 0.486	62.3
(174050) 2002 CC19	OASI	2021/02/04	17.644 ± 0.697	6.2

Table A1 – *continued*

Asteroid	Observatory	Date	mag	α (°)
	OASI	2021/02/04	17.834 ± 0.427	6.8
	OASI	2021/02/04	17.835 ± 0.428	7.1
	OASI	2021/02/05	18.284 ± 0.076	11.9
	OASI	2021/02/09	18.780 ± 0.600	28.6
	OASI	2021/02/11	18.913 ± 0.671	35.4
(175189) 2005 EC224	CI	2017/03/17	18.10 ± 0.03	0.7
	CI	2017/03/17	18.22 ± 0.03	0.8
	CI	2017/03/17	18.30 ± 0.03	0.8
	CI	2017/03/16	18.24 ± 0.03	1.3
	CI	2017/03/16	18.28 ± 0.03	1.4
	CI	2017/03/19	18.26 ± 0.04	1.4
	CI	2017/03/19	18.38 ± 0.03	1.5
	OASI	2017/03/21	18.33 ± 0.113	3.1
	OASI	2017/03/23	18.398 ± 0.266	4.7
	OASI	2017/03/24	18.424 ± 0.099	5.6
	OASI	2017/03/25	18.512 ± 0.094	6.5
	OASI	2017/03/26	18.592 ± 0.11	7.3
	OASI	2017/03/27	18.626 ± 0.101	8.2
	CI	2017/03/28	18.76 ± 0.03	9.0
	CI	2017/03/29	18.61 ± 0.05	9.8
	CI	2017/03/30	18.71 ± 0.03	10.7
	CI	2017/04/03	18.96 ± 0.05	13.3
	CI	2017/04/13	19.17 ± 0.03	22.6
	CI	2017/04/22	19.32 ± 0.04	29.3
	OASI	2020/05/17	18.889 ± 0.075	23.1
	OASI	2020/05/26	19.075 ± 3.433	28.0
	OASI	2020/06/20	19.383 ± 0.083	36.4
	OASI	2020/06/21	19.331 ± 0.146	36.6
(417581) 2006 VA3	OASI	2021/02/04	17.832 ± 0.391	11.4
	OASI	2021/02/05	17.872 ± 0.111	12.7
	OASI	2021/02/05	17.798 ± 0.080	13.0
	OASI	2021/02/11	18.136 ± 0.343	26.3
	OASI	2021/03/13	19.941 ± 0.395	81.0
(464797) 2004 FZ1	OASI	2016/08/27	18.078 ± 0.084	8.7
	OASI	2016/08/29	18.049 ± 0.051	12.2
	OASI	2016/08/29	18.131 ± 0.053	12.3
	OASI	2016/08/31	18.413 ± 0.218	15.5
	OASI	2016/09/01	18.190 ± 0.126	17.2
	OASI	2016/09/01	18.242 ± 0.121	17.4
	OASI	2016/09/02	18.369 ± 0.157	18.7
	OASI	2016/09/02	18.408 ± 0.131	18.9
(480004) 2014 KD91	OASI	2016/10/07	17.867 ± 0.358	14.8
	OASI	2016/10/04	17.858 ± 0.106	18.5
	OASI	2016/10/02	17.889 ± 0.451	20.4
	OASI	2016/10/02	17.947 ± 0.480	20.5
	OASI	2016/09/29	18.171 ± 0.270	23.1
	OASI	2016/09/28	18.042 ± 0.265	23.8
	OASI	2016/09/28	18.128 ± 0.293	23.9
	OASI	2016/09/27	18.143 ± 0.313	24.6
	OASI	2016/09/27	18.052 ± 0.652	24.7
2011 YQ10	OASI	2021/12/01	19.184 ± 0.576	5.7
	OASI	2021/12/07	19.041 ± 0.296	7.9
	OASI	2021/10/07	20.475 ± 0.452	47.0
	OASI	2021/10/03	20.257 ± 0.108	48.1
	OASI	2021/10/01	20.342 ± 0.790	48.3
2016 RP33	OASI	2016/09/24	19.468 ± 0.083	7.6
	OASI	2016/09/24	19.613 ± 0.077	7.7
	OASI	2016/09/25	19.627 ± 0.143	9.0
	OASI	2016/09/25	19.602 ± 0.109	9.1
	OASI	2016/09/25	19.648 ± 0.100	9.2
	OASI	2016/09/26	19.811 ± 0.411	10.5
	OASI	2016/09/27	19.872 ± 0.346	11.9
	OASI	2016/09/27	19.642 ± 0.258	12.0
	OASI	2016/09/27	19.696 ± 0.254	12.1

Table A1 – *continued*

Asteroid	Observatory	Date	mag	α (°)
	OASI	2016/09/28	19.903 ± 0.228	13.3
	OASI	2016/09/29	19.877 ± 0.233	14.6
	OASI	2016/10/02	20.090 ± 0.436	18.2
	OASI	2016/10/02	19.985 ± 0.397	18.3
2017 AC5	CI	2017/03/16	20.414 ± 0.169	5.4
	CI	2017/03/02	20.549 ± 0.139	8.8
	OASI	2017/03/21	20.591 ± 0.015	9.6
	OASI	2017/03/23	20.670 ± 0.017	11.5
	OASI	2017/03/24	20.915 ± 0.019	12.4
	OASI	2017/03/25	20.630 ± 0.019	13.4
	OASI	2017/03/26	20.969 ± 0.030	14.3
	CI	2017/02/20	20.656 ± 0.109	15.0
	CI	2017/03/27	20.619 ± 0.129	15.3
	CI	2017/03/31	21.115 ± 0.149	18.8

For each asteroid is given: the name, the date, the **corrected** magnitude (mag), and the solar phase angle (α).

Table A2. The determined parameters H-G_1–G_2 for the 30 NEOs used in our analysis.

Asteroid	H_{0R}	H_{0Rerr}	G_1	G_{1err}	G_2	G_{2err}	fit_{err}
(4055) Magellan	13.94	− 1.23 +0.85	0.07041	− 0.0722 +0.0929	0.3724	− 0.335 +0.5273	±0.188
(16816) 1997 UF9	15.39	− 1.00 +1.29	0.0	− 0.0 +0.0849	0.3322	− 0.2336 +0.6034	±0.026
(18109) 2000 NG11	16.53	− 0.08 +0.62	0.8301	− 0.2413 +0.048	0.01628	− 0.0 +0.4196	±0.01
(36236) 1999 VV	115.77	− 0.04 +0.55	0.8228	− 0.0093 +0.0535	0.01938	− 0.0 +0.184	±0.03
(65717) 1993 BX3	20.45	− 0.18 +0.47	0.9662	− 0.3761 +0.0207	0.0	− 0.0 +0.4091	±0.199
(99799) 2002 LJ3	18.21	− 0.46 +0.22	0.7792	− 0.1462 +0.0182	0.2208	− 0.2539 +0.1456	±0.07
(159608) 2002 AC2	15.79	− 1.03 +0.7	0.1234	− 0.1271 +0.1583	0.2317	− 0.1773 +0.4871	±0.29
(163693) Atira	15.7	− 0.08 +0.39	0.8238	− 0.0268 +0.0564	0.0	− 0.0188 +0.1703	±0.529
(174050) 2002 CC19	16.626	− 0.234 +0.241	0.0	− 0.0 +0.0731	0.1919	− 0.0475 +0.0655	±0.377
(175189) 2005 EC224	18.07	− 1.14 +0.179	0.3626	− 0.0 +0.1679	0.343	− 0.0 +0.480	±0.0148
(326683) 2002 WP	18.05	− 1.39 +0.88	0.0	− 0.0 +0.5503	0.6025	− 0.0709 +0.1939	±0.048
(333889) 1998 SV4	17.69	− 0.39 +0.60	0.7062	− 0.2324 +0.1227	0.1075	− 0.0264 +0.4447	±0.079
(370307) 2002 RH52	16.41	− 0.84 +0.94	0.0	− 0.0 +0.2763	0.5726	− 0.0359 +0.4111	±0.226
(370702) 2004 NC9	17.05	− 0.94 +0.57	0.8187	− 0.8128 +0.1872	0.1813	− 0.0381 +0.8084	±0.101
(417581) 2006 VA3	17.37	− 0.41 +0.21	0.7687	− 0.2397 +0.2298	0.2313	− 0.0273 +0.2346	±0.055
(464797) 2004 FZ1	17.39	− 0.92 +0.62	0.2593	− 0.0693 +0.3836	0.3831	− 0.0405 +0.2917	±0.091
(480004) 2014 KD91	16.96	− 0.36 +0.67	0.2613	− 0.007 +0.0534	0.3499	− 0.0056 +0.136	±0.425
(480824) 1999 JO6	16.37	− 0.08 +0.57	0.8072	− 0.2139 +0.0	0.0	− 0.0494 +0.3808	±0.13
(484506) 2008 ER7	20.0	− 0.93 +0.4	0.629	− 0.6264 +0.3611	0.371	− 0.0693 +0.5748	±0.057
(489337) 2006 UM	16.45	− 0.16	0.1515	− 0.0152	0.0	− 0.0502	±0.41

Downloaded from https://academic.oup.com/mnras/article/523/1/739/7165783 by Biblioteca do Conj. das Químicas-USP user on 23 August 2023

Table A2 *– continued*

Asteroid	H_{0R}	H_{0Rerr}	G_1	G_{1err}	G_2	G_{2err}	fit_{err}
2001 UG18	20.56	$+1.44$ -0.64	0.4619	$+0.0$ -0.3297	0.3302	$+0.4548$ -0.0594	±0.009
2005 TF	18.84	$+0.55$ -1.16	0.06187	$+0.3148$ -0.1111	0.1475	$+0.4306$ -0.0851	±0.529
2011 YQ10	18.844	$+1.32$ -0.3	0.6749	$+0.1366$ -0.2069	0.3251	$+0.7147$ -0.0093	±0.12
2014 AD17	19.67	$+0.29$ -1.15	0.2481	$+0.2388$ -0.0	0.3532	$+0.2049$ -0.0658	±0.188
2016 WJ1	20.98	$+0.42$ -0.56	0.2588	$+0.2576$ -0.1026	0.3721	$+0.3348$ -0.0019	±0.01
2016 WU3	20.06	$+0.06$ 0.40	0.8228	$+0.2946$ -0.0838	0.01938	$+0.1134$ -0.0665	±0.051
2016 RP33	18.331	$+0.96$ -0.619	0.1609	$+0.0803$ -0.0291	0.1418	$+0.5153$ -0.1288	±0.229
2017 AC5	20.01	$+0.603$ -1.25	0.819	$+0.0414$ -0.057	0.0	$+0.2355$ -0.0	±0.326
2017 CR32	22.33	$+1.47$ -0.48	0.8571	$+0.0$ -0.5498	0.133	$+0.9755$ -0.0589	±0.031
2017 DC38	24.22	$+1.13$ -0.50	0.8017	$+0.3161$ -0.4329	0.0	$+0.5839$ -0.0273	±0.08
		$+0.88$		$+0.0$		$+0.62$	

For each asteroid is given: the name, the H_{0R} and associated error, the G_1 value, the G_1 error, the G_2, the G_2 error and the fit error (*fit*$_{err}$).

This paper has been typeset from a TeX/LaTeX file prepared by the author.

© 2023 The Author(s)
Published by Oxford University Press on behalf of Royal Astronomical Society